Laguerre-Gauss Preprocessing:
Line Profiles as Image Features for Aerial Images Classification

Alejandro Murillo-González
Universidad EAFIT
amurillog@eafit.edu.co

José David Ortega Pabón
Fuerza Aérea Colombiana
jose.ortega@fac.mil.co

Juan Guillermo Paniagua
Universidad EAFIT
juanpaniagua@itm.edu.co

Olga Lucía Quintero Montoya
Universidad EAFIT
oquinte1@eafit.edu.co

Abstract

An image preprocessing methodology based on Fourier analysis together with the Laguerre-Gauss Spatial Filter is proposed. This is an alternative to obtain features from aerial images that reduces the feature space significantly, preserving enough information for classification tasks. Experiments on a challenging data set of aerial images show that it is possible to learn a robust classifier from this transformed and smaller feature space using simple models, with similar performance to the complete feature space and more complex models.

1. Introduction

Image preprocessing techniques aim to enhance an image's relevant features and suppress those that are considered noise for the task at hand [23]. This process involves transforming the representation, usually a matrix filled with intensity values, following a predefined procedure. The desire to obtain an enhanced or smaller representation comes from different areas such as medical diagnosis, information transmission and compression, digital photography and computer vision (CV).

An effective preprocessing might result in the solution of CV problems with simple learning algorithms. This simple models make a more efficient use of the data, which means a time reduction during inference and training, something that is crucial for real-time applications or problems that require online learning. Also, the memory and disk space footprint is reduced. It is important to note that simpler solutions are easier to interpret most of the time, resulting in models whose inner workings are clearer.

Therefore, this work explores the applicability of procedures that reduce an image's feature space to perform classification tasks using k-Nearest Neighbors (kNN) [5] and Multilayer Perceptrons (MLP) [17; 8], which are models currently displaced -in this task- by more powerful but expensive models such as Convolutional Neural Networks (CNN) [11; 8].

The employed approach is based on spectrum analysis tools, particularly Fourier analysis. It uses the Laguerre-Gauss Spatial Filter (LGSF), as kernel, proposed by Gou *et al.* [9], who state that "it allows the realization of a radial Hilbert transform with high contrastive and isotropic edge enhancement without resolution loss". This means that the borders will be intensified (in all directions), thus making them easier to detect. In [3] the authors compare LGSF against other common edge enhancing technique (Laplacian filtering) and found it to be superior given that it acts as a bandpass reducing low and high frequency noise, and that it "distributed homogeneously and smoothly the intensity of the magnitude of the Fourier spectrum due to its isotropic feature". The latter statements are an indication that a line profile, along an axis of an image preprocesed with this filter, will result in a coherent curve. Is this line profile, taken along the x- and y-axis, that will be used in this work as the feature space during classification. Furthermore, the results from Sierra-Sosa *et al.* [21] showed that, after Double Fourier analysis, the line profile of a voiced speech was useful to classify emotions.

Using the feature space obtained from the principles described above, it was possible to obtain good performance on multiple classification tasks such as Geometric Shapes and Aerial Images, where CNN were replaced by kNN and MLP. As a preliminary result, this preprocessing methodology could be extended to other CV tasks.

Concretely, the contribution of this paper is the description of an image preprocessing methodology to reduce the dimensionality of the data and perform classification with simple models. Particularly, a challenging data set of Aerial

Images will be classified using this method.

The code implementation of Laguerre-Gauss Preprocessing and the presented results is available on GitHub [1].

The remaining of this article is organized as follows. Section 2 gives an overview of the related work. Section 3 goes over the preliminary theoretical framework. In Section 4 the proposed methodology for image feature space reduction and classification is described. Section 5 presents the data sets employed and the results obtained. Section 6 discusses the results. Finally, Section 7 introduces the reached conclusions.

2. Related Work

Line Profiles. Sierra-Sosa *et al.* [21] use Fourier analysis on spectrograms of audio recordings to identify the speaker's emotions using the spectrum's line profile. In [7] multiple line profiles, whose position are based on maxima in the Hough transform space, are used to recognize logos (classification over invariant classes). In [15] the authors employ line intensity profiles to identify reflections in eye images, which are then classified as reflections or non-reflections using a suport vector machine. Bhan *et al.* [1] use feature line profiles from preprocessed radiographic images to detect dental caries and their severity.

The works described above, specially those on images, work over very restricted spaces. In the Aerial Images classification task the environments and elements of each class have higher variation.

Aerial Images. In [26; 14] the authors propose CNNs to detect objects from aerial images. Qayyum *et al.* [13] use CNN to classify scenes in aerial images extracting features in multiple scales which are then encoded into global image features.

3. Preliminaries

This section introduces the definitions and theorems (based on [6]) behind Laguerre-Gauss Preprocessing, which is described in Section 4.

3.1. Integral Transforms

Def. An *Integral Transform* is defined as

$$\mathcal{I}\{f(\mathbf{x})\} = F(\mathbf{k}) = \int_s \mathcal{K}(\mathbf{x}, \mathbf{k}) f(\mathbf{x}) d\mathbf{x} \quad (1)$$

where $\mathbf{x} = (x_1, x_2, \ldots, x_n), \mathbf{k} = (k_1, k_2, \ldots, k_n), S \subset \mathbb{R}^n$ and $\mathcal{K}$ is the kernel of the transform. The *inverse transform* is an operator such that

$$\mathcal{I}^{-1}\{F(\mathbf{k})\} = f(\mathbf{x}) \quad (2)$$

3.1.1 Convolution

Def. The *Convolution* of two integrable functions $f(\mathbf{x})$ and $g(\mathbf{x})$, denoted by $(f * g)(\mathbf{x})$, is

$$(f * g)(\mathbf{x}) = \int_{-\infty}^{\infty} f(\mathbf{x} - \xi) g(\mathbf{x}) d\xi \quad (3)$$

Convolution Theorem. If $\mathcal{I}\{f(\mathbf{x})\} = F(\mathbf{k})$ and $\mathcal{I}\{g(\mathbf{x})\} = G(\mathbf{k})$, then

$$\mathcal{I}\{f(\mathbf{x}) * g(\mathbf{x})\} = F(\mathbf{k})G(\mathbf{k})$$
$$f(\mathbf{x}) * g(\mathbf{x}) = \mathcal{I}^{-1}\{F(\mathbf{k})G(\mathbf{k})\} \quad (4)$$

Furthermore, commutativity, associativity and distributivity is valid under a convolution.

3.1.2 Fourier Transform

A particular case of an integral transform is the Fourier transform which turns a function's (signal) time domain into its frequency representation.

Def. The *Multiple Fourier Transform* of $f(\mathbf{x})$, where $\mathbf{x} = (x_1, x_2, \ldots, x_n)$ is the *n*-dimensional vector, is defined by

$$\mathcal{F}\{f(\mathbf{x})\} = \frac{1}{(2\pi)^{\frac{n}{2}}} \int_{-\infty}^{\infty} \cdots \int_{-\infty}^{\infty} \exp\{-i(\mathbf{k} \cdot \mathbf{x})\} f(\mathbf{x}) d\mathbf{x} \quad (5)$$

where $\mathbf{k} = (k_1, k_2, \ldots, k_n)$ is the *n*-dimensional vector, $\mathbf{k} \cdot \mathbf{x} = k_1 x_1 + k_2 x_2 + \cdots + k_n x_n$ and $f(\mathbf{x})$ is absolutely integrable.

3.2. Hilbert Space

Def. Let $\mathcal{H}$ be a vector space. A bi-linear mapping $< \cdot, \cdot >: \mathcal{H} \times \mathcal{H} \to \mathbb{R}$ is an *inner product* if it satisfies symmetry, linearity and positive definiteness.
Def. A vector space $\mathcal{H}$ is a *Hilbert space* if it is a complete inner product space.
Def. Given a Hilbert space $\mathcal{H}$, a *feature mapping* $\phi : x \to \mathcal{H}$ is a function such that $\phi(x) \in \mathcal{H}$.
Theorem. Any feature mapping defines a valid kernel.

Note that having a Hilbert space enables transformations in any number of dimensions. Once a kernel is obtained, a transformation, as defined in 1, can be performed using it.

3.3. Laguerre-Gauss Spatial Filter (LGSF)

The LGSF is the kernel employed during preprocessing to enhance the edges and reduce low- and high- frequency noise [9; 3].

The filter, proposed by Guo *et al.* [9], in the spatial domain is given by [12]

$$LG(x, y) = (i\pi^2\omega^4)(x + iy) \exp\{-\pi^2\omega^2(x^2 + y^2)\} \quad (6)$$

where ω is a parameter that controls the bandpass filter size. As ω approaches 1 it favors higher frequencies, that is, thinner edges.

3.4. Line Profile

The line profile of a matrix is the sampling of its values along a path.

This work uses the line profiles taken along a line segment that crosses the origin and is parallel to the $x-$ and $y-$axis.

In the case of images in the spatial domain, the line profile samples the intensity value of its pixels. If the image is in the frequential domain, the line profile samples a frequency, which is a complex number z. To visualize the sampled frequencies it is possible to take the amplitude (which is the absolute value of z), its phase, its real or its imaginary component.

4. Proposed Method
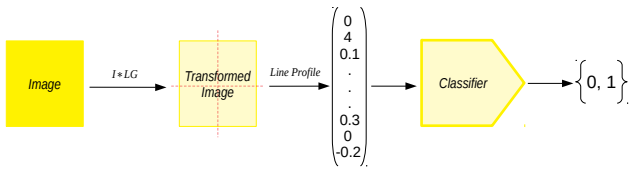
Figure 1. Overview of Laguerre-Gauss Preprocessing.

4.1. Overview

Figure 1 summarizes the Laguerre-Gauss preprocessing procedure. The methodology is based in the application of integral transforms as described in Section 3.1. It acts on a function to produce another simpler representation. This might also happen to be interpretable and enable comparison between other functions who undergone the same transformation process.

Particularly, this transformation process involves getting the Fourier's spectrum representation from the image $\hat{I}$ and the LGSF $\hat{LG}$ filter introduced in Section 3.3. Once both analytic signals are obtained, given that they are no longer in the spatial domain, their convolution is their point-wise multiplication $I * LG = \hat{I} \cdot \hat{LG}$. Here LG is acting as a feature mapping, therefore it is considered a valid kernel, as seen in Section 3.2.

The remaining steps involve shifting the zero-frequency components to the center of the image to obtain an image whose origin is at its center. Then the line profiles are sampled along the $x-$ and $y-$axis.

This procedure means that if an image of size $n \times n$ is being classified, the classifier will only need $2 \times n$ features, reducing significantly the feature space.

4.2. Laguerre-Gauss Preprocessing

In order to reduce the model's dimensionality, the input images will be preprocessed to obtain a set of features representative of the elements present on it.

Preprocesssing is as follows:

1. Create the Laguerre-Gauss filter [12] from equation 6 with the same size as the image and a given ω. It is usually set to $\omega = 0.9$ to better distinguish the image's borders.

2. Apply Fourier's transform to the filter and the image.

3. Once the analytic signal of both the filter and the image is obtained, they are convolved. This is done through element-wise multiplication. Since the filter is 2-dimensional, the images should be transformed to one channel (i.e., grayscale) or apply the filter to each or a set of channels on a channel-wise basis.

4. Next, the zero-frequency components are shifted to the center of the spectrum. This means that the origin of the image will be its center.

5. Finally, the x and y line-profiles are obtained from the shifted image. This is the vector representing the spectrum along the origin in the $x-$ and $y-$ axis respectively.

Algorithm 1 presents the pseudocode of the Laguerre-Gauss Preprocessing procedure.

Algorithm 1: Laguerre-Gauss Preprocessing

Data: image, ω
s $\leftarrow$ size(image);
filter $\leftarrow$ LaguerreGaussFilter(ω, s);
image$_{FT}$ $\leftarrow$ FourierTransform(image);
filter$_{FT}$ $\leftarrow$ FourierTransform(filter);
convolved $\leftarrow$ image$_{FT}$ $\cdot$ filter$_{FT}$;
shifted $\leftarrow$ shift(convolved);
x-profile $\leftarrow$ LineProfile($shifted, axis = x$);
y-profile $\leftarrow$ LineProfile($shifted, axis = y$);
return x-profile, y-profile

---

5. Results

This section describes the data set and classifiers employed, together with the results from using each of them with Laguerre-Gauss preproprocessing, and without it. Also, it presents the results from a couple of ablation experiments to show the utility of this preprocessing methodology as a whole.

5.1. Data Sets

5.1.1 Geometric Shapes

This data set is a mix of [19; 10; 18; 25] which combines computer generated and hand-drawn geometric shapes. All images are resized to 64×64 pixels. Basically, the images are monochromatic with different sizes, rotations and deformations. Specifically, the shapes to be classified are Circles (which includes ellipses), Squares (which includes rectangles) and Triangles. Table 1 shows the data set specificities.

Set	Circles	Squares	Triangles	Total
Train	3277	4058	3608	10943
Validation	859	803	720	2382
Test	889	847	600	2336

Table 1. Description of Geometric Shapes data set.

5.1.2 Aerial Images

This data set was collected to identify illegal mining and deforestation in large areas. The images come from multiple news agencies [2; 16; 20; 24] which have covered this phenomena. The idea is to classify an image in the class 1 if it contains something of interest (i.e., heavy-equipment, boats, deforestation, etc.); or as class 0 if it does not (i.e., forest, rivers, populations, etc.). The data set contains 5707 instances (resized to 64×64 pixels) of which 3297 (57% of the total) images are samples of class 0 and the remaining are samples from class 1. The data was augmented to 20000 instances through random rotations ($\pm 20°$, $90°$, $270°$), left-to-right and top-to-bottom flips.

The main challenge posed by this data set is the infinite number of possible camera angles and altitudes from which the images are taken. Also, the noise added by images from moving cameras, fog, clouds and changing climates. Note that not all images come from the same distribution, since they are taken in different locations with different kinds of sensors.

5.2. Classification

Three kinds of learners (kNN, MLP & CNN) were used to test the preprocessing methodology against no-preprocessing, or a flattened representation of an image.

The **kNN** employed a value of $k = 1$ for the number of neighbors in all tasks.

The **MLP** used the *same* architecture for all tasks (regardless of the data representation), therefore the results reported here might be improved with custom-made architectures. The MLP featured an input layer with 128 units, two hidden layers with 64 and 32 units respectively, and an output layer with as many units as the number of classes in the problem. For regularization, a dropout layer was embedded

after each of the three initial layers, with probability 0.5, 0.25 and 0.25, respectively.

The **CNN** also used the *same* architecture for all tasks. The architecture is shown in Figure 2. It was chosen from [4], such that it had an excellent performance on MNIST, therefore the results for other data sets might be improved with different architectures.

Finally, both the MLP and CNN used categorical crossentropy as loss and RMSProp as optimizer. Also, all their layers used relu as activation function, except the last one which used softmax. No hyper-parameter tuning took place.

5.2.1 Geometric Shapes

Table 2 presents the classification results using three kinds of models (kNN, MLP and CNN). It describes the scores obtained using a flattened representation of the image's pixel intensities matrix and compares it with the classification scores using Laguerre-Gauss Preprocessing (LP). A quick glance returns that the classifiers using LP did better, except in the case of CNN, but considering the disk space trade-off and the inference time, the MLP might be a better option for real-time and embedded applications, since the score's difference is minimal.

Figure 5 shows the mean line profiles for the train instances of the geometric shapes. From it is possible to see the differences in the frequency spectrum within the different shapes; this differences can also be appreciated by the learners.

5.2.2 Aerial Images

The results of the classification of aerial images are reported on Table 3. There it is possible to see that the MLP using the flattened representation of the image cannot break the class imbalance as the accuracy never goes above 57%, which is confirmed by the F1 score. On the other hand, the MLP using the LP representation does really well on the data set obtaining around 80% accuracy. It is remarkable the size difference of this model with the other ones tested. In the case of the kNN implementation, even though the flattened representation has slightly better performance, its size might be a constraint when deploying on resource constrained environments. The huge difference in size is due to the fact that kNN need to store the support seen during training, as a result a smaller feature space, such as LP, will inevitably result in a smaller and faster model.

Figures 3 and 4 show the Receiver Operating Characteristic (ROC) curve of the kNN and MLP models employing the LP feature space. The results displayed on the figures are a good indication of the combined precision and recall of the models.

Figure 6 shows the mean line profiles for the classes in the data set. Here, similar to the case of geometric shapes, the differences in the frequency spectrum are observable, allowing the models to learn them too.

The CNN from Figure 2 cannot break the class imbalance, therefore its results on the task are not reported.

| 2D Convolution |
| Kernel: 3x3 – Filters: 128 |
| 2D Convolution |
| Kernel: 3x3 – Filters: 64 |
| Max Pool |
| Kernel: 2x2 |
| Dropout |
| Probability: 0.25 |
| Flatten |
| Dense |
| Units: 32 |
| Dropout |
| Probability: 0.5 |
| Dense |
| Unit: # classes |
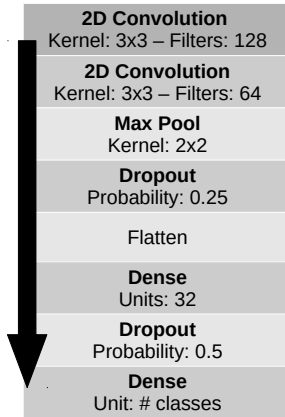
Figure 2. CNN Architecture employed for the classification tasks.

5.3. Ablation Study

This section describes a couple of changes to the Laguerre-Gauss preprocessing procedure in order to better understand how each component affects the process of reducing the feature space. Even though the procedure contains more than two steps, the steps tested here are the ones that are theoretically allowed, since direct modifications of the filter, or with it, would not make sense.

Tables 4 and 5 show the accuracy and F1 scores after removing the convolution and shift step during preprocessing, respectively.

5.3.1 Convolution

This step consists of ignoring the convolution of the Fourier transform of the image with the Fourier transform of the filter. Instead, the Fourier transform of the image is calculated and the procedure remains unmodified, but uses this transformed representation.

From Table 4 it seems that removing this step is actually good. This could be an effect of the lack of background noise in this images, where the object to classify is not hidden by others. But on Table 5 the performance is degraded on MLP. Also, note that while training, the model quickly reaches the reported accuracy and the loss stops decreasing, meaning that the network has stopped learning and started over-fitting.

5.3.2 Unshifted Components

Here, once the image is convolved the line profiles are directly calculated assuming that the center of the image is the axis' origin. Basically, the convolution is not rearranged and the frequency components are disorganized across the matrix.

From Table 4 it is possible to see that removing this step greatly degrades geometric shape classification performance. On Table 5 the performance is also diminished. The main differences are reported by the F1 score.

6. Discussion

The introduced methodology can learn a robust classifier for Aerial Images and Geometric shapes (see Tables 2 and 3). Particularly for the Aerial Images, the model faces many challenges given the diverse set of characteristics present in the images.

As shown in [12] the LGSF can avoid noise in the image by ignoring the low- and high- frequencies. Furthermore, once the Fourier transform of an image is computed, the random noise (usually white noise) behaves as a constant in the Fourier frequency domain [22]. Also as seen in Section 3.2 the transform is linear so the "data transform is the sum of the signal and noise transforms" [22]. This feature might give robustness to adversarial attacks, but was not tested in this paper.

As stated in Section 4, the parameter ω of the LGSF was fixed to 0.9, as a trade-off between prioritizing high frequencies (sharper edges) but being conscious of the importance of lower frequencies, specially in images taken at high-altitudes, where the objects in the surface are difficult to detect. The selection of this hyper-parameter according to the characteristics of each data set (through hyper-parameter tuning) should return better models. Specifically, for the Aerial Images, upon inspection of the misclassified instances (in train, validation and test data sets), it was seen that most errors occurred on images taken from high-altitudes, meaning that the classifier is constrained to certain altitudes.

Additionally, since this methodology extracts features of the images from the frequency domain it can be expected that it can generalize to diverse environments, since it does not need to know its particularities (i.e., background noise: deserts, ocean, etc.), and instead can look for relevant shapes. In [21] they hypothesize a similar result on emotion recognition from different languages. Overall, this will mean a more robust classifier.

Figures 5 and 6 show the average line profile for the training data. From them it is clear that they differ the most around the center of the spectrum. Since both data sets were resized to images of size 64×64 the spectral resolution is truncated. Determining an adequate spectral resolution

Model	Data	Size	Train		Validation		Test	
			Accuracy	F1	Accuracy	F1	Accuracy	F1
kNN	Flattened	750.8 MB	-	-	0.9513	0.94/0.94/0.96	0.9601	0.95/0.95/0.97
	LP	**23.7 MB**	-	-	**0.9832**	0.97/0.98/0.99	**0.9880**	0.98/0.98/0.99
MLP	Flattened	4.4 MB	0.9661	0.95/0.95/0.98	0.9311	0.93/0.90/0.95	0.9066	0.90/0.88/0.94
	LP	**374.7 kB**	**0.9770**	0.96/0.97/0.98	**0.9563**	0.94/0.95/0.97	**0.9563**	0.95/0.95/0.96
CNN	Image	15.5 MB	**0.9819**	0.98/0.97/0.98	0.9550	0.95/0.93/0.97	0.9584	0.96/0.94/0.96

Table 2. Results of Geometric Shape classification. The shapes are a combination of hand-drawn and computer generated with different sizes. The F1 score is reported for each class in the next order: Circle, Square, Triangle.

Model	Data	Size	Train		Validation		Test	
			Accuracy	F1	Accuracy	F1	Accuracy	F1
kNN	Flattened	951.2 MB	**0.9257**	0.93/0.91	**0.9286**	0.93/0.91	**0.9183**	0.92/0.90
	LP	**30.0 MB**	0.9030	0.91/0.88	0.8900	0.90/0.86	0.9046	0.9151/0.89
MLP	Flattened	4.4 MB	0.5747	0.72/0.0	0.5720	0.72/0.0	0.5730	0.72/0.0
	LP	**376.4 kB**	**0.8012**	0.82/0.76	**0.8116**	0.83/0.77	**0.7990**	0.82/0.76

Table 3. Results of Aerial Images classification. The F1 score is reported for each class in the next order: 0 - No object of interest / 1 - object of interest.

(higher or lower) means that a better model could be obtained; in the case of Aerial Images, from the average line profiles, it can be seen that the line profiles could be truncated to obtain an even smaller feature space and still have differentiating characteristics. This results particularly interesting for classification tasks with many labels and variance within elements of the same class. For instance, Smith and Gray [22] say that line profiles differ the most at larger frequencies, where noise is even smaller. The latter confirms that images of higher resolution might return a better feature space.

Following on the topic of line profiles, their value lies in the fact that for different classes it is possible to obtain peaks and valley of varying amplitudes and at different frequencies. Since the synthesized profiles obtained in this work always lied in the axis, it remains necessary to study how sampling profiles from other paths within the spectrum might help to obtain a richer feature space.

Regarding the ablation study, the convolution step turned out to be relevant for classification of Aerial Images. When tested on Geometric Shapes, its effect is counterproductive. This is an important fact, given that it supports the LGSF as a good edge enhancer (which was not needed on Geometric Shapes, since they already had their edges clearly defined). On the other side, the shifting phase turned out to be really important when constructing the reduced feature space. This confirms that specific edge directions describe most of the images and a feature space where every time different directions are sampled does not provide value.

An application where this methodology can be successfully applied is finding regions of interest within large areas/images. Due to the simple models, inference on partitions of the image will quickly return those places where a more expensive model should focus, avoiding the costs of running it over the whole space.

7. Conclusion

This work introduced Laguerre-Gauss Preprocessing. It was shown that it can be successfully applied to robustly learn to classify aerial images with simple models. As a result, the models size footprint is reduced, as well as the training and inference time. The LGSF enabled edge enhancement and reduced the low- and high-frequency noise. The LGSF distributes homogeneously and smoothly the intensity in the Fourier spectrum due to its isotropic feature. This resulted in characteristic frequencies that allowed learning special/relevant shapes within an image. In addition, The LGSF can enhance any small changes in the image according to small changes in frequency.

The parameter ω tends to one in order to preserve the spatial frequency distribution in the image and perform the bandpass filter component from the LGSF, but it is important to analyze and propose a methodology to select the appropriate value depending on each data set.

This feature selection technique achieves models with a lower complexity (measured in terms of the VC dimensionality) and introduces a tool to develop a robust, quick, simplified and low-cost solution which can be deployed in aerial vehicles.

Future work could focus on extending this method for classification tasks with more categories where the shapes have high variance between elements of the same class.
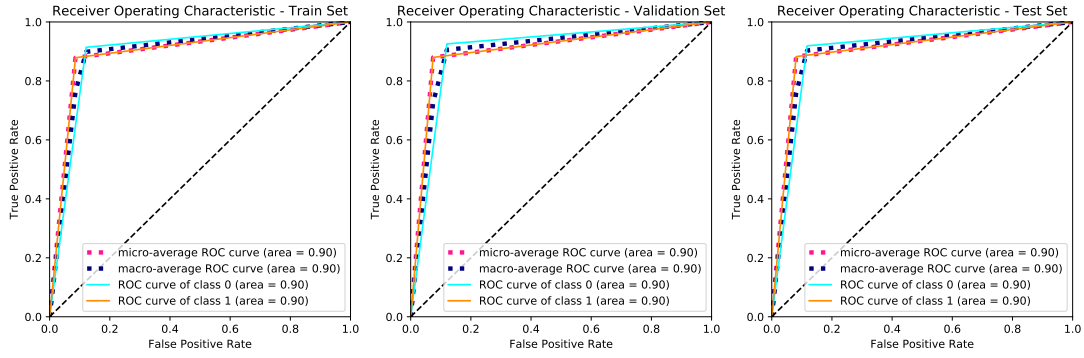
Figure 3. ROC curve for a kNN trained to classify Aerial Images.
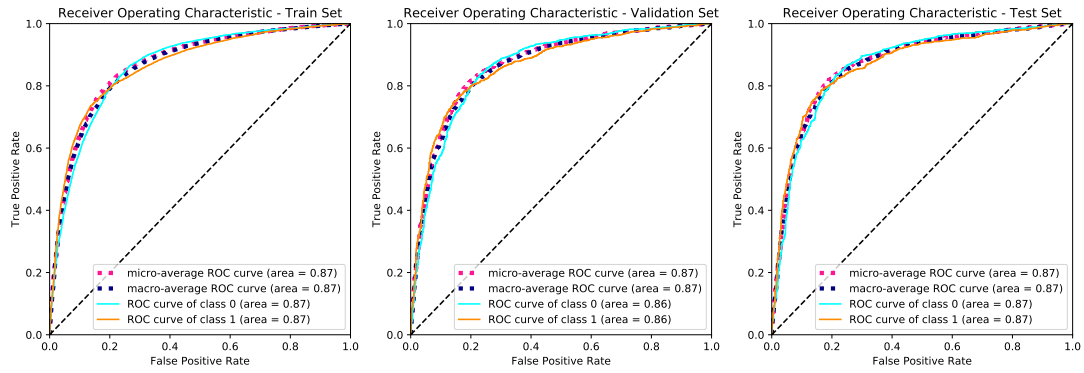
Figure 4. ROC curve for a MLP trained to classify Aerial Images.

Model	Removed Step	Train		Validation		Test	
		Accuracy	F1	Accuracy	F1	Accuracy	F1
kNN	Convolution	-	-	0.9840	0.97/0.98/0.99	0.9888	0.98/0.98/0.99
	Shift	-	-	0.8400	0.82/0.85/0.84	0.6519	0.70/0.58/0.67
MLP	Convolution	0.9966	0.99/0.99/0.99	0.9857	0.98/0.98/0.99	0.9884	0.98/0.98/0.99
	Shift	0.5919	0.63/0.33/0.75	0.5780	0.64/0.27/0.73	0.6078	0.70/0.39/0.67

Table 4. Ablation test on Geometric Shapes.

Model	Removed Step	Train		Validation		Test	
		Accuracy	F1	Accuracy	F1	Accuracy	F1
kNN	Convolution	0.9048	0.91/0.88	0.9053	0.91/0.88	0.9120	0.92/0.89
	Shift	0.8770	0.89/0.85	0.8806	0.89/0.85	0.8850	0.90/0.86
MLP	Convolution	0.7478	0.77/0.72	0.7606	0.78/0.72	0.7490	0.77/0.71
	Shift	0.7411	0.78/0.66	0.7520	0.79/0.68	0.7433	0.78/0.67

Table 5. Ablation test on Aerial Images.
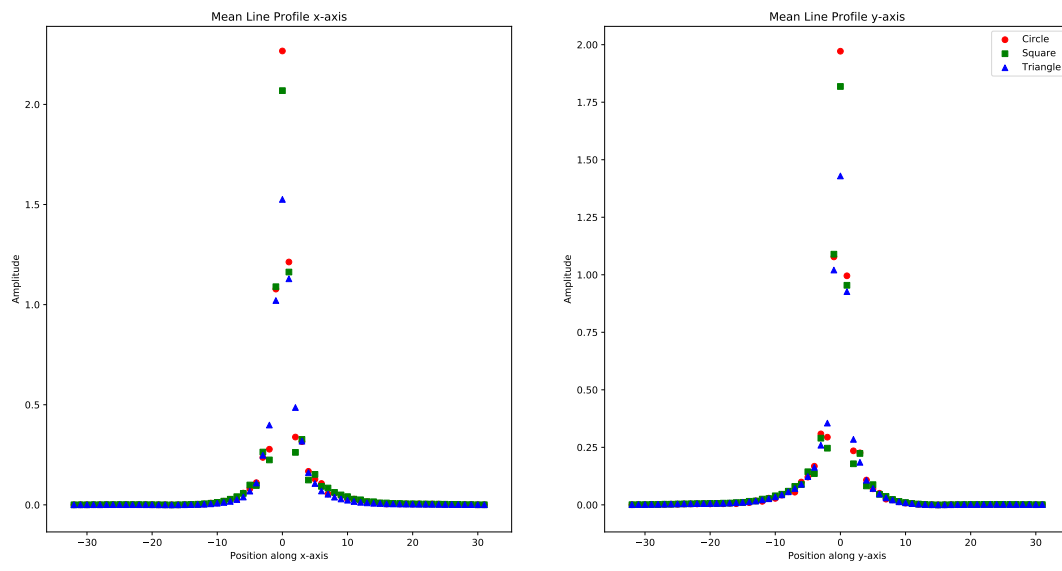
Figure 5. Mean Line Profile Geometric Shapes.
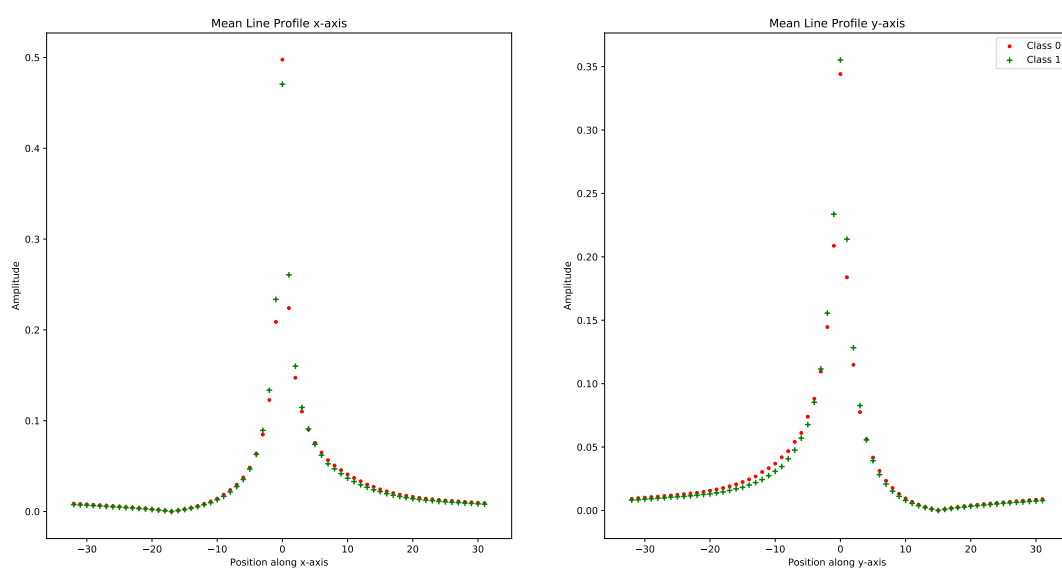
Figure 6. Mean Line Profile Aerial Images.

References

[1] A. Bhan, A. Goyal, Harsh, N. Chauhan, and C. Wang. Feature line profile based automatic detection of dental caries in bitewing radiography. In *2016 International Conference on Micro-Electronics and Telecommunication Engineering (ICMETE)*, pages 635–640, Los Alamitos, CA, USA, sep 2016. IEEE Computer Society.

[2] Noticias Caracol. https://noticias.caracoltv.com/, 2019.

[3] Juan Guillermo Paniagua Castrilln, Olga Lucia Quintero Montoya, and Daniel Sierra-Sosa. Laguerre-gauss filters in reverse time migration image reconstruction. *Brazilian Journal of Geophysics*, 35(2):81–93, 2018.

[4] François Chollet et al. Keras. https://keras.io, 2015.

[5] T. Cover and P. Hart. Nearest neighbor pattern classification. *IEEE Trans. Inf. Theor.*, 13(1):21–27, Sept. 1967.

[6] L. Debnath and D. Bhatta. *Integral Transforms and Their Applications, Second Edition*. Taylor & Francis, 2006.

[7] Richard J. M. den Hollander and Alan Hanjalic. Logo recognition in video by line profile classification. In Minerva M. Yeung, Rainer W. Lienhart, and Chung-Sheng Li, editors, *Storage and Retrieval Methods and Applications for Multimedia 2004*, volume 5307, pages 300 – 306. International Society for Optics and Photonics, SPIE, 2003.

[8] Ian Goodfellow, Yoshua Bengio, and Aaron Courville. *Deep Learning*. MIT Press, 2016. http://www.deeplearningbook.org.

[9] Cheng-Shan Guo, Yu-Jing Han, Jian-Bo Xu, and Jianping Ding. Radial hilbert transform with laguerre-gaussian spatial filters. *Opt. Lett.*, 31(10):1394–1396, May 2006.

[10] Fede Herz. simple shapes. https://www.kaggle.com/fhernand23/simple-shapes/metadata, 2019.

[11] Alex Krizhevsky, Ilya Sutskever, and Geoffrey E Hinton. Imagenet classification with deep convolutional neural networks. In F. Pereira, C. J. C. Burges, L. Bottou, and K. Q. Weinberger, editors, *Advances in Neural Information Processing Systems 25*, pages 1097–1105. Curran Associates, Inc., 2012.

[12] Juan Paniagua and Olga Quintero. Attenuation of reverse time migration artifacts using laguerre-gauss filtering. 06 2017.

[13] Abdul Qayyum, Aamir Saeed Malik, Naufal M Saad, Mahboob Iqbal, Mohd Faris Abdullah, Waqas Rasheed, Tuan AB Rashid Abdullah, and Mohd Yaqoob Bin Jafaar. Scene classification for aerial images based on cnn using sparse coding technique. *International Journal of Remote Sensing*, 38(8-10):2662–2685, 2017.

[14] Matija Radovic, Offei Adarkwa, and Qiaosong Wang. Object recognition in aerial images using convolutional neural networks. *Journal of Imaging*, 3(2):21, Jun 2017.

[15] Anis Farihan Mat Raffei, Hishammuddin Asmuni, Rohayanti Hassan, and Razib M. Othman. Fusing the line intensity profile and support vector machine for removing reflections in frontal rgb color eye images. *Information Sciences*, 276:104 – 122, 2014.

[16] Noticias RCN. https://noticias.canalrcn.com/, 2019.

[17] F. Rosenblatt. The perceptron: A probabilistic model for information storage and organization in the brain. *Psychological Review*, pages 65–386, 1958.

[18] Ruhshan. Geometric-shapes. https://www.kaggle.com/ruhshan/geometricshapes/metadata, 2018.

[19] Mark s. 300 images of squares, circles, and triangles. https://www.kaggle.com/cactus3/basicshapes/metadata, 2018.

[20] Revista Semana. https://www.semana.com/, 2019.

[21] D. Sierra-Sosa, M. Bastidas, D. Ortiz P., and O.L. Quintero. Double fourier analysis for emotion identification in voiced speech. *Journal of Physics: Conference Series*, 705:012035, apr 2016.

[22] M. A. Smith and D. F. Gray. Fourier analysis of spectral line profiles - a new tool for an old art. *Publications of the Astronomical Society of the Pacific*, 88:809, dec 1976.

[23] Milan Sonka, Vaclav Hlavac, and Roger Boyle. *Image preprocessing*, pages 56–111. Springer US, Boston, MA, 1993.

[24] Periodico El Tiempo. https://www.eltiempo.com/, 2019.

[25] Nachiket Watane. Four shapes. https://www.kaggle.com/nachiket10/four-shapes/metadata, 2018.

[26] I. evo and A. Avramovi. Convolutional neural network based automatic object detection on aerial images. *IEEE Geoscience and Remote Sensing Letters*, 13(5):740–744, May 2016.